# Structural, Electrical and Magnetic Properties of the Co-Substituted Bi-2212 System Textured by Laser Floating Zone Technique

A.Özaslan[a], B. Özçelik[a*], B. Özkurt[b], A. Sotelo[c], M. A. Madre[c]

[a] Department of Physics, Faculty of Sciences and Letters, Çukurova University. 01330 Adana, Turkey

[b] Department of Electronic and Computer Education, Faculty of Tarsus Technical Education, University of Mersin, Mersin/Turkey

[c] ICMA (CSIC-Universidad de Zaragoza). María de Luna, 3. 50018 Zaragoza, Spain.

## ABSTRACT

In this work, $Bi_2Sr_2CaCu_{2-x}Co_xO_y$ (x =0.0, 0.05, 0.10, and 0.25) textured superconductors were prepared by a LFZ melting technique. In all cases, the powder X-ray diffraction patterns of samples show that Bi-2212 phase is the major one. All samples have good oriented structure, which is a typical picture for superconductors prepared by LFZ method. Magnetization hysteresis loops, made for all samples at two different temperatures, showed that the loops become narrower with increasing temperature and doping levels. In addition, the effect of Co doping on the critical current density, $J_C$, of $Bi_2Sr_2CaCu_{2-x}Co_xO_y$ has been estimated from hysteresis loop measurement by using Bean's model. The increase of Co amount in $Bi_2Sr_2CaCu_{2-x}Co_xO_y$ structure significantly decreases the critical current density, showing worse connectivity of the grains. All the results indicate that Co substitution for Cu produces the deterioration on the superconducting properties, compared with the undoped samples.

***Keywords:*** Bi-based cuprates, XRD, SEM, Critical Current, M-H, LFZ-technique

***Corresponding Author:** Tel./fax:+90.322.3386060/2496/+90.322.3386070

**e-mail:** *ozcelik@cu.edu.tr*

## 1. Introduction

The Bi-based superconductor [1] family is composed of three different phases described by the $Bi_2Sr_2Ca_{n-1}Cu_n O_{2n+4+y}$ general formula, where n =1, 2 and 3. Moreover, n is related to the number of $CuO_2$ layers in the crystal structure, producing the well-known Bi-2201, 2212 and 2223, respectively, with 20, 85, and 110 K critical temperatures for each one [2-4]. Since the discovery of high-*Tc* superconductivity in the BSCCO system [1], intense studies have been performed [5-22] in order to improve its critical temperature (*Tc*), critical current density (*Jc*), and better understand the structural properties of the system. One of the useful methods, in this regard, is the substitution of rare-earths elements at different cationic sites. Rare-earth substitution leads to important changes in charge carrier concentration and also releases the restriction of spin alignment due to the spin lattice interaction [23]. The effect of such changes is one of the important features that help understanding the structural details and superconducting properties along with the mechanism of occurrence of superconductivity [24-26]. Among the high *Tc* superconductors, Bi-based superconductors are extensively used in the fabrication of wires and tapes due to their layered crystal structure, chemical stability and manufacturing flexibility. Hence, since high temperature superconductors like Bi-base possess a high anisotropy from the crystallographic point of view but also from the transport one texturing techniques can be used to improve their electrical properties. Due to the Bi-based superconductor's crystal anisotropy, grain orientation and connectivity play an important role on the transport properties and, as a consequence, many different texturing processes have been widely studied. When BSCCO materials are properly textured, their transport properties are improved, in an important manner, compared with the non-textured materials. The texturing methods can be roughly divided into solid state methods, where the sample is maintained as a solid [27,28] and those where the sample is totally molten (directional solidification techniques). Among these last methods, the Laser Floating Zone (LFZ) one has been demonstrated to be an effective technique to produce a good grain orientation not only in Bi-2223 [29,30] and Bi-2212 [22,31] superconductors, but also in other anisotropic systems [32]. This method produces very high thermal gradients in the solidification front, producing a preferential alignment of grains with their c-axis perpendicular to the growth direction [33], maximizing the transport properties in the direction parallel to the growth axis.

In our previous works, we have studied the effect of lanthanides like Yb substitution for Cu [34] and Ce substitution for Ca [35]. Besides the lanthanides, we have also aimed to investigate the effect of transition elements in the BSCCO system. Therefore, in this study, we

have investigated the effects of Co substitution for Cu in Bi-2212 textured ceramics prepared by using the LFZ technique. The X-ray powder diffraction, SEM, dc resistivity and magnetic hysteresis measurements were used to characterize the prepared samples. All samples showed diamagnetic behavior and a nearly sharp drop while passing from *Tc* (onset) to *Tc* (offset). However, the superconducting properties of samples weaken with increasing Co doping level.

## 2. Experimental details

$Bi_2Sr_2CaCu_{2-x}Co_xO_y$ samples, with x =0, 0.05, 0.1 and 0.25 Co additions have been prepared, by a polymer matrix route [20,36], from $Bi(CH_3COO)_2$ (≥99.99%, Aldrich), $Sr(CH_3COO)_2•0.5H_2O$ (99%, Panreac), $Ca(CH_3COO)_2•2H_2O$ (98%, Alfa Aesar), $Cu(CH_3COO)_2•H_2O$ (98%, Panreac) and $Co(CH_3COO)_2·H_2O$ (99.9%, Alfa Aesar) commercial powders. They were weighed in stoichiometric amounts and dissolved in a mixture of glacial acetic acid ($CH_3COOH$) (Panreac PA) and distilled water. The use of a mixture of glacial acetic acid and water is due to the fact that in one side Sr acetate is insoluble in concentrated acetic acid and, on the other side; Bi acetate is not soluble in water [37]. Once obtained a clear blue solution, polyethylenimine (PEI) (Aldrich, 50 wt% water) solution in distilled water, in order to reduce the viscosity of commercial PEI, was added. The mixture becomes dark blue immediately due to the formation of Cu-N coordination bonds. The solution was then introduced into a rotary evaporator to reduce its volume (~80%) followed by heating on a hot plate at about 100 ºC for total solvent evaporation, producing a thermoplastic dark blue paste. Further heating at around 350 ºC produces a decomposition step, as described schematically elsewhere [38]. The resulting powder was then milled in an agate mortar and calcined twice at 750 and 800°C for 12 h in order to decompose the alkaline-earth carbonates in order to avoid the bubbles formation in the melting process.

The prereacted homogeneous powders were used to prepare cylindrical precursors, 120 mm long and 3 mm in diameter, approximately, by cold isostatic pressing with an applied pressure of 200 MPa during 1 minute. The obtained cylinders were used as feed in a directional solidification process performed in a laser floating zone melting (LFZ) installation which has been described schematically in previous works [39]. The cylinder bars have been processed using a continuous power Nd:YAG laser ( $\lambda$ = 1064 nm), under air, using a growth rate of 15 mm/h and a relative rotation of 18 rpm between the seed and feed. After the texturing process, long (more than 15 cm) and dimensionally homogeneous rods have been obtained. These textured rods are composed of different secondary phases due to the incongruent melting of

Bi-2212 [40]. As a consequence, the resulting rods were thermally treated in order to produce the Bi-2212 superconducting phase. This process was performed under air, and consisted in two steps: 60 h at 860 ºC, followed by 12 h at 800 ºC and, finally, quenched in air to room temperature.

In order to identify the present phases in the textured materials, powder X-ray diffraction diagrams of the final products were recorded at room temperature using a Rigaku D/max-B powder diffractometer system working with CuKα radiation and a constant scan rate between $2\theta = 3\text{-}60^{o}$ at room temperature. Calculations of the unit cell parameters were done by using Jade 6.0+ crystal refinement program including Rietveld analysis. The uncertainty of the calculation remained in the ±0.00001 range. SEM micrographs were taken using a LEO Evo-40 VPX scanning electron microscope (SEM) fitted with an energy dispersive spectrometry (EDS) analysis system. Electrical measurements were performed by the conventional four-point probe configuration on about 30 mm long samples. Magnetic measurements were carried out in a 7304 model Lake Shore Vibrating Sample Magnetometer (VSM) system after cooling the sample in zero magnetic field (ZFC) between ±5 kOe at two different temperatures; 10 and 15 K. The $Bi_2Sr_2CaCu_{2-x}Co_xO_y$ samples with x = 0.0, 0.05, 0.1, and 0.25 will be hereafter named as A, B, C, and D, respectively.

## 3. Results and discussion

### 3.1 XRD characterization

Powder XRD patterns for all samples are represented in Fig. 1. From these graphs, it is easily seen that all samples contain the Bi-2212 phase (diffraction peaks indicated by a +) as the major one, independently of the Co substitution amount. Moreover, small amounts of secondary phase ($CaCuO_2$) labeled by a * were observed. The crystal symmetry of all the samples is found to be a tetragonal structure. The lattice parameters have been calculated, using the least squares method, for all samples and the obtained values are presented in Table 1. As it can be deduced from these data, *a-b* parameters, associated to the in-plane Cu-O bond length, increase when Co is added while c-parameter continuously decreases when Co content is raised. These variations are due to the fact that the insertion of $Co^{3+}$ (tending to six-fold coordination) substituting $Cu^{2+}$ ions (with five-fold coordination) in the structure produces a rearrangement of Ca and Sr ions, changing their places in the crystal structure to allow six-fold coordination for the added Cr [41]. These processes lead to the modification on the

oxygen content, producing the reduction in the *c*-parameter and, consequently, the raise in the *a*-*b* parameters. Furthermore, no Co-containing phase is detected, indicating that Co atoms are incorporated into the crystal structure of Bi-2212 superconductor [42-44]. On the other hand, the XRD patterns are very similar for all the samples with only some differences in the relative intensity found in some diffraction peaks which can be produced by an induced orientation of the plate-like grains during sample preparation for XRD experiments.

### 3.2 SEM analysis

SEM images corresponding to longitudinal polished sections of samples grown at 15 mm/h after annealing are displayed in Fig. 2. As discussed previously, the XRD patterns of the samples did not change considerably when Co was added. However, these micrographs present different contrasts, indicating that different phases (identified by EDS) can be found in the bulk material. In Fig.2, three different contrasts can be observed which have been associated to Bi-2212 (grey contrast, #2), Bi-2201 (light grey, #3), in agreement with the XRD data, and CaO (dark grey, #1) not detected in the XRD probably due to its small proportions. These three phases are appearing in all the samples, independently of the Co content. Moreover, a new contrast appears when Co is added, identified as a medium grey one (#4 in Fig.2d) which is present in all the Co-substituted samples. This new phase also shows a Bi-2212 composition where all the added Co can be found substituting Cu in different proportions which are increased when the added Co is raised. The evidence found with the EDS analysis is in clear agreement with the small difference in the ionic radius of both elements (Co and Cu) which allows the substitution in the crystal structure. Moreover, it has been found in previous works in similar systems [45] that Cu can easily substitute Co in the crystal structure. On the other hand, from SEM images it can be clearly seen that the grain alignment is increased with Co content as well as the Co-substituted Bi-2212 proportion. These results confirm that the growth speed, in the LFZ processing of the samples, as well as the annealing temperatures and times, have been adequate to obtain well textured Bi-2212 as major phase, independently of the Co doping values.

### 3.3 Electrical measurements

The electrical resistivity (ρ) versus temperature (T) curves obtained for all samples are plotted in Fig. 3 from 130 K down to 5 K. In this figure, it can be clearly seen that samples A, B, and C posses a very similar behavior over *Tc* (onset) transition, with a metallic-like behavior, while sample D shows a semiconducting-like one. Under the superconducting *Tc* (onset)

transition temperatures, the ρ(T) curves show typical characteristics of common Bi-2212 superconductors in all tested samples, which have a relatively sharp decreasing after *Tc* (onset) transition temperatures. On the other hand, the *Tc* (offset) transition temperature values decrease significantly with increasing Co concentration (see Table 1). This trend in transition temperature values indicates the lower superconducting properties of the system with increasing Co concentration. In addition, the *Tc* (offset) transition temperature value was found to be considerably decreased compared with pure sample. It reveals important changes in hole concentration values (see Table 1). The onset critical ($T_c^{onset}$) and offset critical ($T_c^{offset}$) temperatures obtained from the normalized resistance graph versus Co-content are illustrated in Fig.4. It can be easily seen that both critical temperatures gradually decrease with the increase of Co amount and the difference between them is increased. These effects can be easily explained by the magnetic properties of Co ions which is detrimental for the spin-singlet state of Cooper pairs since the exchange field of the ferromagnetic Co aligns the spin of electrons [46,47].

3.4 Carrier concentration calculation

The number of holes, p, per Cu atom can be calculated by using the relation

$$\frac{T_c}{T_c^{\max}} = 1 - 82.6(p - 0.16)^2$$

given by Presland *et al.* [48], where $T_c^{\max}$ is taken as 85 K for the Bi-2212 system and $T_c^{offset}$ values are taken from Table 1. The results obtained show that the p-values of the samples range from 0.145 to 0.057 (see Table 1). The number of the hole-carrier concentrations is in agreement with previously reported results by Bal *et al.* [49]. The variation of hole-concentration as a function of Co-content is displayed in Fig.5. As can be seen, the hole-concentration decreases with increasing Co substitution. This is due to the fact that $Co^{3+}$ is substituting $Cu^{2+}$ leading to the increase of oxygen content which is expected to decrease the superconducting properties of the system.

3.5 Magnetic properties

The magnetic-hysteresis cycles, between applied fields of ± 6 kOe, for all the samples, at 10 and 15 K, are shown in Figs. 6 and 7, respectively. The magnetic-hysteresis loops of the samples shows that the magnitude of magnetization effectively depends on Co doping levels. There is a clear reduction of magnetization volume in the entire range of magnetic fields for

all samples when Co content is increased, *i.e.* the hysteresis loops are getting narrower with increasing doping Co-content and temperature. In addition, the diamagnetic behavior observed in the M-H loops of all samples except for x = 0.25 sample confirms the occurrence of a conventional type-II superconductors. There is no measurable volume in the magnetic-hysteresis loop for the x = 0.25 sample, indicating that this sample has nearly paramagnetic properties as shown in the inset of fig.6. These effects can be explained using the arguments described previously in the electrical measurements section. Moreover, they are confirmed with the SEM observations which show an increase of the Co-substituted Bi-2212 phase when Co content is raised. As a consequence of the higher amount of the Co-doped phase, the Cooper pair breaking is increased and the magnetic properties diminish.

From these data, the *Jc* values of the samples were determined using the Bean's model [50];

$$Jc = 30\,\Delta M / d\,,$$

where *Jc* is the magnetization current density in ampéres per square centimeter of a sample. $\Delta M = M+ - M-$ is measured in electromagnetic units per cubic centimeter, and *d* is the thickness of sample.

Figure 8 shows the critical current density value at 10 K estimated from M-H loops for all samples up to 6 kOe. Calculated *Jc* of all samples effectively decreased for H > 500 Oe with the increasing of magnetic field and Co contents. The important decrease in the *Jc* values for the Co-doped samples studied in this work implies that the resistance to the flux creep of pure sample is greater than that of the others due to the lower superconducting properties of the Co-substituted Bi-2212 phases which do not act as effective pinning centers. It can be also concluded that the field dependence of $J_c$ can be related to the presence of structural defects or the weak links between grains, typical feature in ceramic superconductors.

## CONCLUSIONS

In this study, the effect of Co substitution for Cu on the structural and superconducting properties of Bi-2212 prepared by a by a polymer matrix route and then textured by the LFZ technique has been studied. XRD suggests that samples with nearly single Bi-2212 phase have been obtained, independently of the Co content. The SEM micrographs confirm that all samples are predominantly composed by the Bi-2212 phase and a new Co-substituted Bi-2212 phase when Co is added. R-T results indicated that all samples exhibit metallic behavior over $T_c$ (onset), except for the highest doped one which shows semiconducting one. Moreover, all

samples showed a broad transition from the normal to the superconducting state, pointing out to the presence of impurities and weak links between superconducting grains. From M-H measurements, it has been found that the magnetization values and the volume of the closed hysteresis curves decrease with increasing Co-content, due to the formation of the Co-substituted Bi-2212 phase. Employing Bean's model, it has been found that the increase on Co contents produces a decrease on *Jc* values.

**Acknowledgements**

This work is supported by Research Fund of Çukurova University, Adana, Turkey, under grant contracts no: FEF2012YL7. A. Sotelo and M. A. Madre wish to thank the Gobierno de Aragón (Research Group T12), for financial support. M. A. Madre also acknowledges the MINECO-FEDER (Project MAT2011-22719) for funding.

**References**


[1] Maeda, H.,Tanaka, Y., Fukutumi, M., Asano, T.: Jpn. J. Appl. Phys. 27, L209 (1988)

[2] Gao, L., Huang, J. C., Meng, L. R., Hor, H. P., Bechtold, J., Sun, Y. Y., Chu,W. C., Sheng, Z. Z., Herman, M. A.: Nature 332, 623 (1988)

[3] Chu, W. C., Bechtold, J., Gao, L., Hor, H. P., Huang, J. C., Meng, L. R., Sun, Y. Y., Wang, Y. Q., Zue, Y. Y.: Phys. Rev. Lett. 60,941 (1988)

[4] Tallon, L. J., Buckley, G. R.,Gilbert, W. P.,Presland, R. M., Brown, M. W. I., Bowder, E. M., Christian, A. L., Gafull, R.: Nature 333, 153 (1988)

[5] Coskun, A., Ekicibil, A., Ozcelik, B.: Chin. Phys. Lett. 19/12, 1863 (2002)

[6] Ozkurt, B., Ekicibil, A., Aksan, M. A., Ozçelik, B.,Yakıncı, M. E., Kiymac, K.: J. Low Temp. Phys. 149, 105 (2007)

[7] Yazıcı, D., Ozçelik, B.,Yakıncı, M. E.: J. Low Temp. Phys. 163, 370 (2011)

[8] Sözeri, H., Ghazanfari, N., Özkan, H., Kılıç, A.: Supercond. Sci. Technol. 20, 522 (2007)

[9] Sotelo, A., Mora, M., Madre, M. A., Diez, J. C., Angurel, L. A., de la Fuente, G. F.: J. Eur. Ceram. Soc. 25, 2947 (2005)

[10] Jiang, L., Sun, Y., Wan, X., Wang, K., Xu, G., Chen, X., Ruan, K., Du, J.: Physica C 300, 61 (1998)

[11] Zargar Shoushtari, M., Mousavi Ghahfarokhi, S. E.: J.. Supercond. Nov. Magn. 24, 1505 (2011)

[12] Abou-Aly, A. I., Abdel Gawad, M. M. H., Awad, R., G-Eldeen, I.: J. Supercond. Nov. Magn. 24, 2077 (2011)

[13] Mora, M., Sotelo, A., Amaveda, H., Madre, M. A., Diez, J. C., Angurel, L. A., de la Fuente G. F.: Bol. Soc. Esp. Ceram., 44, 199 (2005)

[14] Şakiroğlu, S., Kocabaş, K.: J. Supercond. Nov. Magn. 24, 1321 (2011)

[15] Khalil, S. M.: J. Phys. Chem. Solids 62 457 (2001)

[16] Sotelo, A., Madre, M. A., Diez, J. C., Rasekh, Sh., Angurel, L. A., Martinez, E.: Supercond. Sci. Technol. 22, 034012 (2009)

[17] Madre, M. A., Amaveda, H., Mora, M., Sotelo, A., Angurel, L. A., Diez, J. C.: Bol. Soc. Esp. Ceram. 47, 148 (2008)

[18] Chen, Y. L., Stevens, R.: J. Am. Ceram. Soc. 75, 1150 (1992)

[19] Ramesh, R., Green, S., Jiang, C., Mei, Y., Rudee, M., Luo, H., Thomas, G.: Phys. Rev. B, Condens. Matter 38, 7070 (1988)

[20] de la Fuente, G. F., Sotelo, A., Huang, Y., Ruiz, M. T., Badia, A., Angurel, L. A., Lera, F., Navarro, R,. Rillo, C., Ibañez, R., Beltran, D., Sapiña, F., Beltran, A.: Physica C 185-189, 509 (1991)

[21] Sotelo, A., Szillat, H., Majewski, P., Aldinger, F.: Supercond. Sci. Technol. 10, 717 (1997)

[22] Özkurt, B., Madre, M. A., Sotelo, A., Yakıncı, M. E., Özçelik, B.: J. Supercond. Nov. Magn. 25, 799 (2012)

[23] Ando, Y., Lavrov, A.N., Komiya, S., Segawa, K., Sun, X.F.: Phys. Rev. Lett. 87:017001 (2001)

[24] Tarascon, J. M.,Barboux, P., Hull, G. W., Ramesh, R., Greene L. H., Gariod, M., Hedge, M. S., Mckinnon, W. R.: Phys. Rev. B 38, 4316 (1989)

[25] Eisaki, H., Kaneko, N., Feng, D., Fengi L., Damascelli, A., Mang, P. K., Shen, Z. X., Greven, M.:Phys. Rev. B 69, 064512 (2004)

[26] Fujita, K., Noda, T., Kojima, K.M., Eisaki, H., Uchida, S.: Phys. Rev. Lett. 95, 097006 (2005)

[27] Garnier, V., Caillard, R., Sotelo, A., Desgardin, G.: Physica C 319, 197 (1999)

[28] Marinel, S., Bourgault, D., Belmont, O., Sotelo, A., Desgardin, G.: Physica C 315, 205 (1999)

[29] Huang, Y. B., de la Fuente, G. F., Sotelo, A., Badia, A., Lera, F., Navarro, R., Ibañez, R., Beltran, D., Sapiña, F., Beltran, A.: Physica C 185-189, 2401 (1991)

[30] Carrasco, M. F., Costa, F. M., Silva, R. F., Gimeno, F., Sotelo, A., Mora, M., Diez, J. C., Angurel, L. A.: Physica C 415, 163 (2004)

[31] Sotelo, A., Mora, M. A., Amaveda, H., Diez, J. C., Angurel, L. A., Mayoral, M. C.: Bol. Soc. Esp. Ceram. V. 45, 228 (2006)

[32] Sotelo, A., Guilmeau, E., Madre, M. A., Marinel, S., Diez, J. C., Prevel, M.: J. Eur. Ceram. Soc. 27, 3697 (2007)

[33] de la Fuente, G. F., Ruiz, M. T., Sotelo, A., Larrea, A., Navarro, R.: Mater. Sci. Eng. A 173, 201 (1993)

[34] Gundogmus H., Özçelik B., Özkurt B., Sotelo, A., Madre, M. A.: J. Supercond. Nov. Magn., 26, 111 (2012),

[35] Kaya C., Özçelik B., Özkurt B., Sotelo, A., Madre, M. A.: J. Mater. Sci.: Mater. Electron. (2012) DOI 10.1007/s10854-012-0979-z

[36] Sotelo, A., Rasekh, Sh., Madre, M. A., Diez, J. C.: J. Supercond. Nov. Magn. 24, 19 (2011)

[37] Lide, D. R.: CRC Handbook of Chemistry and Physics. CRC Press/Taylor and Francis, Boca Raton, FL (2010)
[38] Sotelo, A., Angurel, L. A., Ruiz, M. T., Larrea, A., Lera, F., de la Fuente, G. F.: Solid State Ionics 63-65, 883 (1993)
[39] Mora, M., Sotelo, A., Amaveda, H., Madre, M. A., Diez, J. C., Capel, F., Lopez-Cepero, J. M.: J. Eur. Ceram. Soc. 27, 3959 (2007)
[40] Angurel, L. A., Diez, J. C.,, de la Fuente, G. F., Gimeno, F., Lera, F., Lopez-Gascon, C., Martinez, E., Mora, M., Navarro, R., Sotelo, A., Andres, N., Recuero, S., Arroyo, M. P. Phys. Status Solidi A 203, 2931 (2006)
[41] Tarascon J. M., Ramesh R., Barboux P., Hedge M. S., Hull G. W., Greene L. H., Giroud M.: Solid State Commun. 71, 663 (1989)
[42] Vinu S., Sarun P. M., Biju A., Shabna R., Guruswamy P., Syamaprasad U.: Supercond. Sci. Technol. 21, 045001 (2008)
[43] Vinu S., Sarun P. M., Shabna R., Biju A., Syamaprasad U.: Mater. Lett. 62, 4421 (2008)
[44] Shabna R., Sarun P. M., Vinu S., Biju A., Syamaprasad U.: Supercond. Sci. Technol. 22, 045016 (2009)
[45] Rasekh, Sh., Torres, M. A., Constantinescu, G., Madre, M. A., Diez, J. C., Sotelo, A.: J. Mater. Sci.: Mater. Electron. (2013) DOI: 10.1007/s10854-013-1094-5
[46] Keizer, R. S., Goennenwein, S. T. B., Klapwijk, T. M., Miao, G., Xiao, G., Gupta, A., Nature 439, 825 (2006)
[47] Stampoulos, D., Pissas. M., Phys. Rev. B 73, 132502 (2006)
[48] Presland M. R., Tallon J. L., Buckley R. G., Liu R. S., Floer N. E.: Physica C 176, 95 (1991)
[49] Bal S., Dogruer M., Yıldırım G., Varilci A., Terzioglu C., Zalaoglu Y.: J. Supercond. Nov. Magn. 25, 847 (2012)
[50] Bean C.P.: Phys. Rev. Lett. 8, 250 (1962)

**Table I.** $T_c$ values deduced from the R-T measurement data, unit cell parameters and hole-carrier concentration for each of the sample

| ***Samples*** | ***$T_c$(K)*** | ***$\Delta T$(K)*** | ***Unit-cell parameter a=b ( Å)*** | ***Unit-cell parameter c ( Å)*** | ***Hole number (p)*** |
|---|---|---|---|---|---|
| A | $T_{c.onset}$=101K<br>$T_{c.offset}$=95K | 6 | 3.819 | 30.950 | 0,145 |
| B | $T_{c.onset}$=91K<br>$T_{c.offset}$=84K | 7 | 3.832 | 30.900 | 0,119 |
| C | $T_{c.onset}$=84K<br>$T_{c.offset}$=67K | 17 | 3.832 | 30.939 | 0,099 |
| D | $T_{c.onset}$=26K<br>$T_{c.offset}$=11K | 15 | 3.832 | 30.850 | 0,057 |

**Figure captions**

**Figure 1.** XRD patterns of the A, B, C, and D samples. Peaks corresponding to the Bi-2212 and $CaCuO_2$ phases are indicated by + and *, respectively

**Figure 2.** SEM micrographs of polished longitudinal sections of the $Bi2Sr2CaCu2_{-x}Co_xO_y$ (x= 0, 0.05, 0.1 and 0.25) samples after annealing. The numbers indicate the different phases: (1) CaO; (2) Bi-2212; (3) Bi-2201; and (4) secondary phases with Bi.

**Figure 3.** The electrical resistivity $\rho$ versus temperature T curves for all samples for 0<T<120 K.

**Figure 4.** $T_c^{onset}$ and $T_c^{offset}$ values versus Co-content.

**Figure 5.** Variation of hole-carrier concentration versus Co-content.

**Figure 6.** M-H curves for all samples measured at 10 K.

**Figure 7.** M-H curves for all samples measured at 15 K.

**Figure 8.** Calculated critical current densities, $J_c$, of the samples, as a function of applied field, at 10K.

**Figure 1**

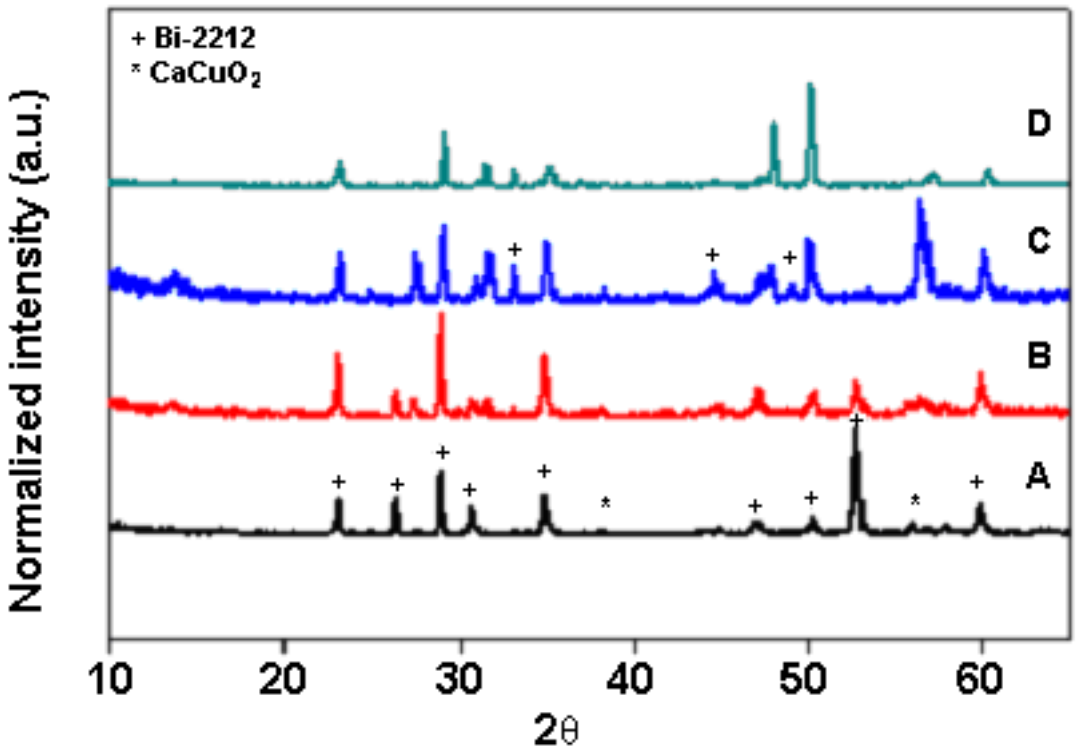
+ Bi-2212
* CaCuO2
D
C
B
A
Normalized intensity (a.u.)
10
20
30
40
50
60
2θ

**Figure 2**

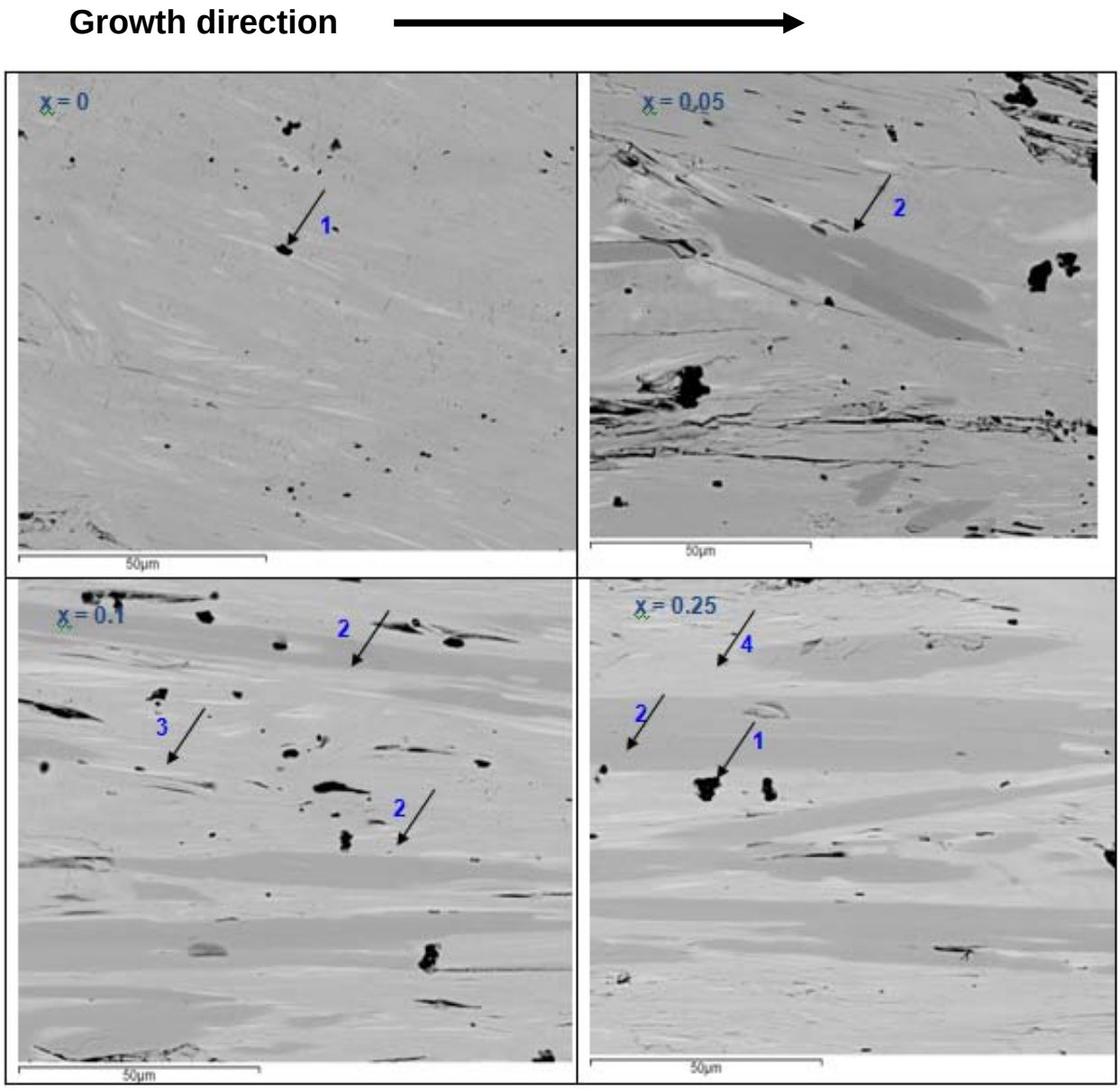
Growth direction
x = 0
1
50µm
x = 0,05
2
50µm
x = 0.1
2
3
2
50µm
x = 0.25
4
2
1
50µm

**Figure 3**

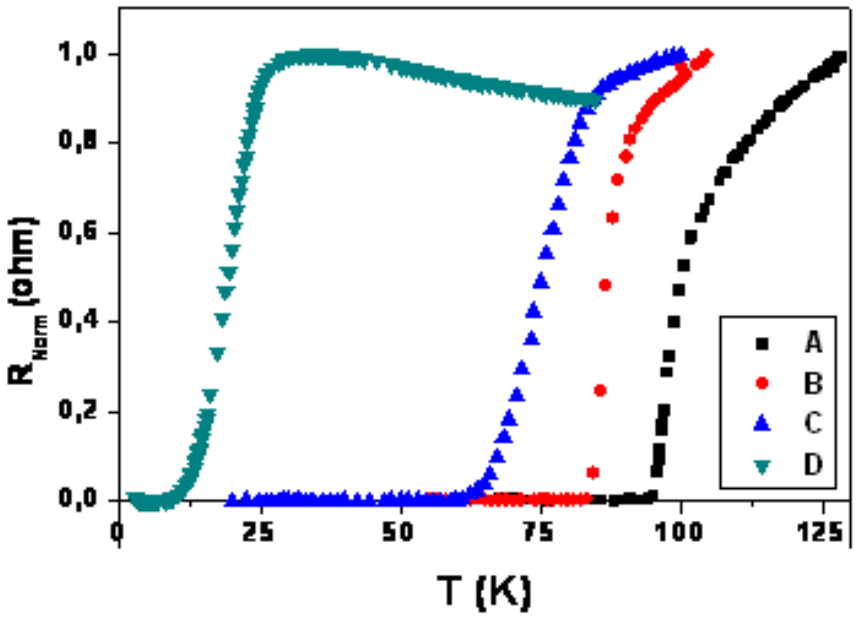

**Figure 4**

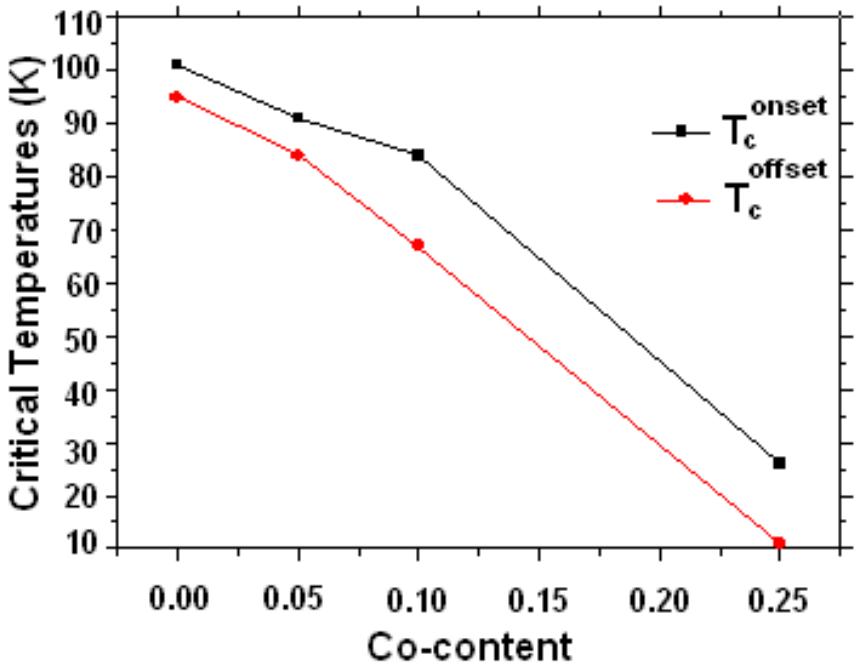
Critical Temperatures (K)
110
100
90
80
70
60
50
40
30
20
10
0.00
0.05
0.10
0.15
0.20
0.25
Co-content
$T_c^{onset}$
$T_c^{offset}$

**Figure 5**

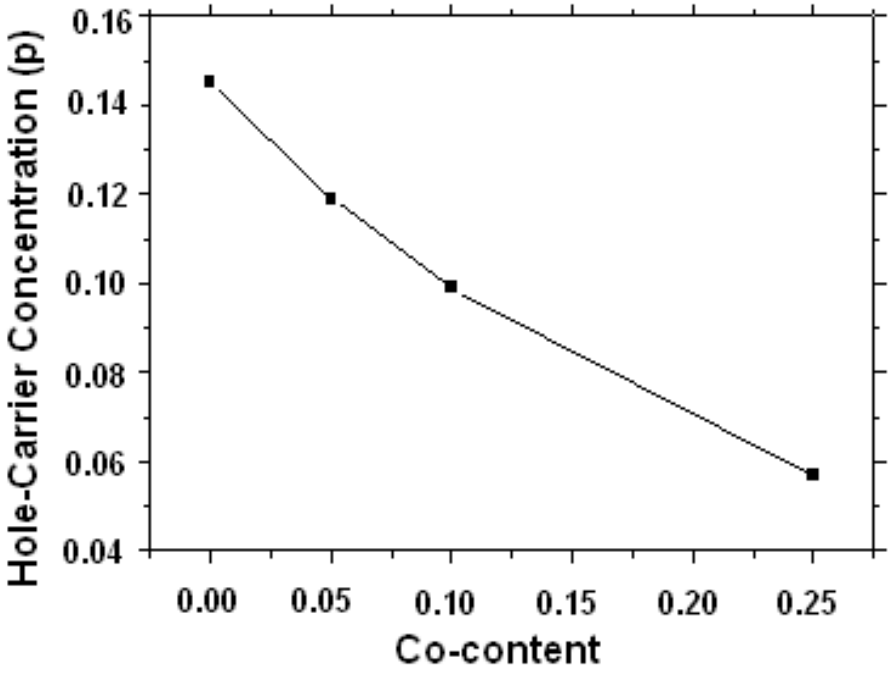
Hole-Carrier Concentration (p)
0.16
0.14
0.12
0.10
0.08
0.06
0.04
0.00
0.05
0.10
0.15
0.20
0.25
Co-content

**Figure 6**

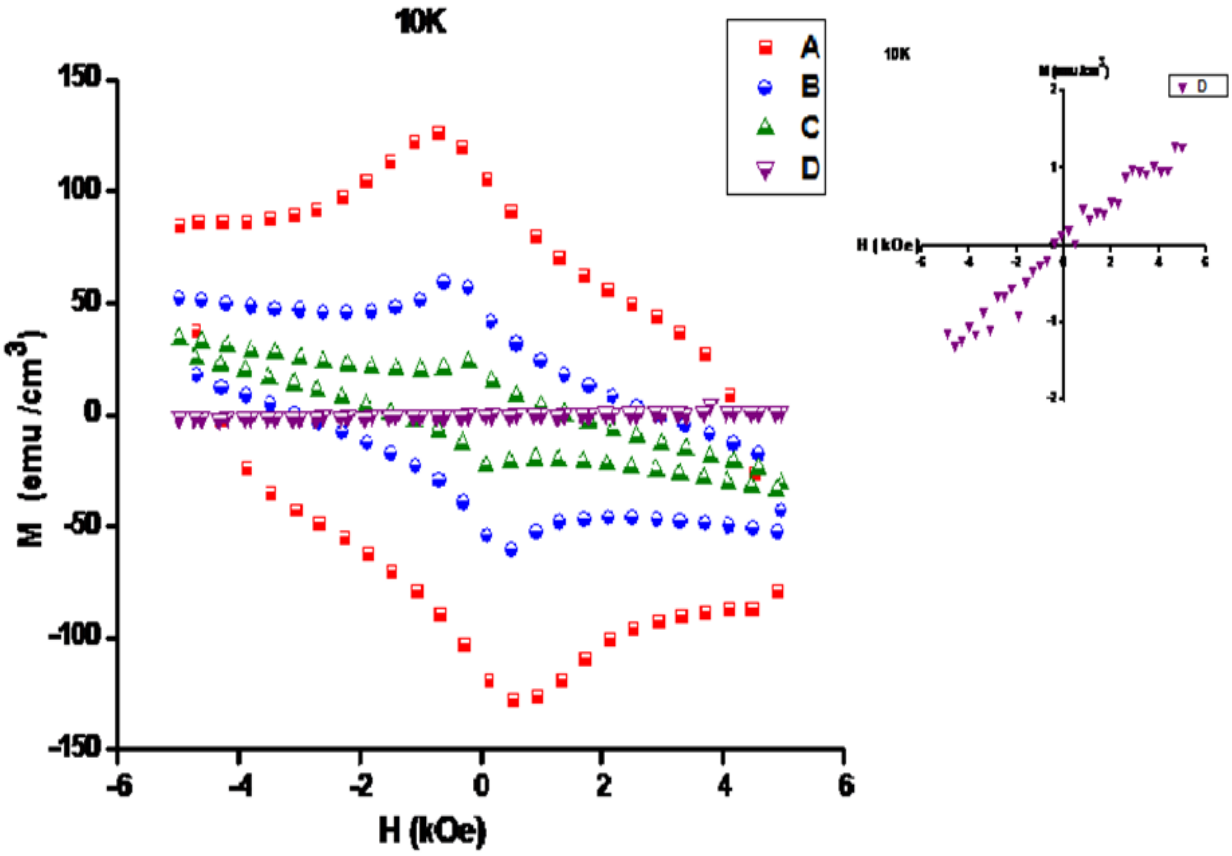
10K
A
B
C
D
M (emu /cm3)
H (kOe)
150
100
50
0
-50
-100
-150
-6
-4
-2
0
2
4
6
10K
D
H (kOe)

**Figure 7**

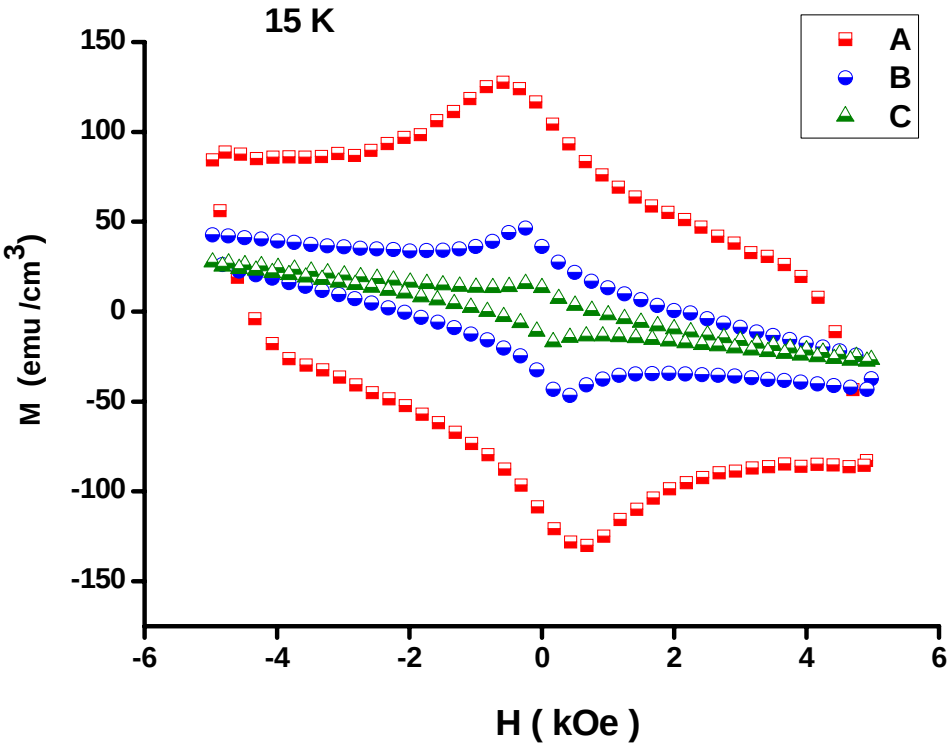

**Figure 8**